

RSC Advances



This is an *Accepted Manuscript*, which has been through the Royal Society of Chemistry peer review process and has been accepted for publication.

Accepted Manuscripts are published online shortly after acceptance, before technical editing, formatting and proof reading. Using this free service, authors can make their results available to the community, in citable form, before we publish the edited article. This *Accepted Manuscript* will be replaced by the edited, formatted and paginated article as soon as this is available.

You can find more information about *Accepted Manuscripts* in the [Information for Authors](#).

Please note that technical editing may introduce minor changes to the text and/or graphics, which may alter content. The journal's standard [Terms & Conditions](#) and the [Ethical guidelines](#) still apply. In no event shall the Royal Society of Chemistry be held responsible for any errors or omissions in this *Accepted Manuscript* or any consequences arising from the use of any information it contains.



Journal Name

ARTICLE

Highly Monodisperse Magnetite/Carbon Composite Microspheres with Mesoporous Structure as High-Performance Lithium-Ion Battery Anodes

Received 00th January 20xx,
Accepted 00th January 20xx

DOI: 10.1039/x0xx00000x

www.rsc.org/

Hyung-Seok Lim^{‡,a}, Daun Kim^{‡,a}, Jun-Ki Hwang^a, Yu-Jeong Kim^a, Yang-Kook Sun^b and Kyung-Do Suh^a

In this study, we propose a fabrication method of highly monodisperse magnetite/carbon ($\text{Fe}_3\text{O}_4/\text{C}$) composite microspheres with a mesoporous structure. Highly monodisperse porous polystyrene (PS) microspheres are synthesized by traditional seeded polymerization. Textural properties of porous PS microspheres can be controlled by using different amounts of diluent. In order to carbonize and introduce ferrous (Fe^{2+}) and ferric (Fe^{3+}) ions into pores of PS microspheres, the sulfonation reaction is carried out using sulfuric acid. Fe_3O_4 nanocrystals are formed into the pores as well as the surface of the sulfonated porous PS microspheres by a simple wet chemical method. The obtained mesoporous structure of $\text{Fe}_3\text{O}_4/\text{C}$ composite microspheres is still retained after heat treatment in nitrogen atmosphere. The homogeneous distribution of Fe_3O_4 nanocrystals in the porous carbon matrix are analyzed through elemental mapping by preparing cross-sections using focused ion beam scanning electron microscopy milling. When the composite electrodes are tested as an anode material in a Li-ion half-cell, the mesoporous $\text{Fe}_3\text{O}_4/\text{C}$ composite microspheres exhibit not only high reversible capacity of 562 mAh g^{-1} after 100 cycles at 1C but also good capacity retention at various current rates (0.1 – 10C) with a high coulombic efficiency of above 99%.

1. Introduction

Lithium-ion batteries (LIBs) have been utilized as a strong rechargeable energy storage system in the portable electronics market because they have the highest energy density among the commercial rechargeable batteries [1-3]. However, their electrochemical performance still does not meet the increasing demands of LIBs as promising power sources in electric vehicles (EVs) and energy storage systems (ESS) [3-5]. For many years, various active materials have been suggested as alternative anode materials to provide higher specific capacity and stable cyclability of LIBs [6-9]. Among these materials, magnetite (Fe_3O_4) has received much attention as a promising anode material for LIBs because of its much higher specific capacity (928 mAh g^{-1}) than that of commercial graphite ($\sim 372 \text{ mAh g}^{-1}$), low cost, natural abundance and non-toxicity [10, 11]. However, Fe_3O_4 anodes cause poor cycle performance in cells because they have problems associated

with agglomeration and severe volume change during lithiation and de-lithiation [12-14]. These problems can partially be solved by fabricating nanostructured- Fe_3O_4 and carbon composites [4, 5, 15, 16]. First, the design of nanostructured- Fe_3O_4 is an effective way to improve the cyclability due to better contact with the electrolyte and the short diffusion length of Li-ions [6, 17]. However, nanostructured- Fe_3O_4 also shows capacity fading because larger sized agglomerates are formed after continuous long cycling. Hence, many researchers have reported nanostructured- $\text{Fe}_3\text{O}_4/\text{carbon}$ composites to overcome this drawback [18]. Although different types of composites have been fabricated using synthesis techniques such as hydrothermal methods [19, 20], it is hard to homogeneously disperse nanosized- Fe_3O_4 in a carbon matrix because of the high-surface energy of nanosized- Fe_3O_4 [11]. Recently, the porous Si/C composite particles exhibit high capacity as well as stable cycling performance, which can be attributed to their existing pores [21]. In the case of carbon composite materials, uniform dispersion of the nanosized active materials in a carbon matrix is a significant factor for improving the electrochemical performance of the cells [15]. In our previous work, we reported the improved cyclability of $\text{Fe}_3\text{O}_4/\text{C}$ composite microspheres fabricated by oil in water (O/W) system with surface-modified Fe_3O_4 nanoparticles. Surface modification of Fe_3O_4 nanoparticles using citric acid induces homogeneous distribution in carbon phase, which can greatly improve long-term cycle performance. However, the $\text{Fe}_3\text{O}_4/\text{C}$

^a Department of Chemical Engineering, College of Engineering, Hanyang University, Seoul, Republic of Korea, 133-791. E-mail: kdsuh@hanyang.ac.kr

^b WCU Department of Energy Engineering, College of Engineering, Hanyang University, Seoul, Republic of Korea, 133-791.

* Corresponding author (kdsuh@hanyang.ac.kr)

‡ These authors contributed equally to this work.

Electronic Supplementary Information (ESI) available: [OM images of synthetic process; SEM images of porous PS microspheres after sulfonation process; SEM images and Raman spectra of the heat-treated SPS microspheres; Voltage profiles of PC-H4 and PC-H7; Cycling and C-rate performance of the bare Fe_3O_4 electrode]. See DOI: 10.1039/x0xx00000x

composite electrode shows approximately 50 % decrease in the capacity from 0.2C to 10C [22]. The reasons for this rate-capability are the polydisperse particle size and nonuniformity of the porosity for the fast transport of both electrons and Li-ions during the continuous cycling. The fabrication method using O/W system could not narrow size distribution and control the porosity of the Fe₃O₄/C composite particles.

Herein, we report an efficient strategy to homogeneously disperse nanosized Fe₃O₄ anodes in carbon phase and enhance the rate-capability. The highly monodisperse Fe₃O₄/porous carbon (Fe₃O₄/PC) composite microspheres are designed for the fast mass- and charge-transfer. The fabrication process of the designed composite microspheres is shown in figure 1. Sulfonated polystyrene microspheres (SPS) having a porous structure are synthesized as a carbon matrix for nanosized-Fe₃O₄ storage. Nanosized-Fe₃O₄ particles are formed in pores of the SPS microspheres with a homogeneous distribution by a wet chemical method using two types of Fe metal precursors. The total Fe₃O₄ content and specific surface area of composite microspheres depend on the total pore volume of porous polymer microspheres. Electrochemical performance measurements demonstrate that the resulting carbonized Fe₃O₄/C composite microspheres exhibit much higher reversible capacity than that of the porous carbon microspheres in addition to excellent cyclability and rate-capability. In particular, SPS having a larger pore volume can contain more nanosized-Fe₃O₄ particles increasing the specific surface area and show higher specific capacity and better capacity retention even at high current rates.

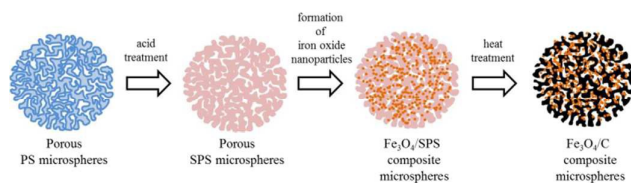


Figure 1. Schematic illustration of the fabrication process of the mesoporous Fe₃O₄/C composite microspheres.

2. Experimental

Mesoporous Fe₃O₄/C composite microspheres were fabricated by heat treatment of mesoporous magnetite/sulfonated polystyrene (Fe₃O₄/SPS) composite microspheres, as shown in figure 1. Highly monodisperse PS microspheres (1.5 μm) with a mesoporous structure were synthesized by seeded polymerization according to the procedure reported in our previous work [23]. After preparation of the mesoporous PS microspheres by seeded polymerization, the particles were sulfonated by acidic treatment with sulfuric acid, and mesoporous Fe₃O₄/SPS composite microspheres were prepared by formation of iron oxide nanocrystals in the porous SPS microspheres. Finally, mesoporous Fe₃O₄/C composite microspheres were obtained by carbonization and pyrolysis of the mesoporous sulfonated PS microspheres.

2.1 Materials

Styrene (St, Sigma-Aldrich) and divinylbenzene (DVB, a mixture of isomers, 55 %, Sigma-Aldrich) were all reagent grade and were used as received. 2, 2'-Azoisobutyronitrile (AIBN, Junsei) and benzoyl peroxide (BPO, Lancaster) were recrystallized to remove an inhibitor from methanol before use. The other materials were used as received without further purification: poly-vinylpyrrolidone (PVP, Mw = 4.0×10⁴ g·mol⁻¹, Sigma-Aldrich), ethanol (Daejung Chemicals & Metals Co., Ltd.), aerosol-OT (AOT, Sigma-Aldrich), polyvinyl alcohol (PVA, Mw = 8.8×10⁴ - 9.2×10⁴ g·mol⁻¹, 87 - 89 % hydrolyzed, Sigma-Aldrich), ammonium hydroxide (25 ~ 28%, Daejung Chemicals & Metals Co., Ltd.), sulfuric acid (95 %, Junsei), sodium lauryl sulfate (SLS, Wako), 1-chlorododecane (CD, TCI), heptane (Daejung Chemicals & Metals Co., Ltd.), iron(II) chloride tetrahydrate (Wako) and iron(III) chloride anhydrous (SHOWA). All aqueous solutions were prepared using distilled (DI) water.

2.2 Preparation of Linear Polystyrene Seed Particles

Linear polystyrene (LPS) seed particles were prepared by conventional dispersion polymerization. St (12.5g), AIBN (0.125g), PVP (1.8g), AOT (0.2g) and ethanol (85g) were mixed homogeneously into a 250 mL four-neck glass reactor equipped with a mechanical stirrer, a refluxing condenser and a nitrogen inlet system. The polymerization reaction was carried out at 70 °C for 24 h with a stirring speed of 120 rpm. The produced LPS seed particles were centrifuged for 10 min at 3600 rpm. After centrifugation, the supernatant solution was decanted, and the remaining LPS seed particles were repeatedly washed with several centrifugations in ethanol and DI water. Finally, the LPS seed particles were dried under a vacuum at room temperature.

2.3 Preparation of Highly Monodisperse Polystyrene Microspheres with a Mesoporous Structure

Highly monodisperse-porous polystyrene (PS) microspheres having different total pore volumes, surface area and average pore size were prepared by seeded polymerization with different amounts of diluent. First, LPS seed particles were dispersed by mechanical stirring and applying ultrasonication in a 0.25 wt. % SLS water/EtOH (5/1, g/g) solution (SE solution) using a 250 ml four-necked glass reactor. The CD emulsions, which were mixed by applying ultrasonication in a SE solution, were poured into the seed dispersion. Stirring speed and temperature were fixed at 200 rpm and 30 °C throughout the swelling process. After the complete diffusion of the CD emulsion into the seed particles, the second monomer mixture of St (7g), DVB (3g), and different amounts of diluent (heptane, 4g and 7g) and BPO (1 wt. % based on monomer) was emulsified and then poured into the mixture containing the CD-swollen seed particles, followed by stirring for 5 h. The swollen particles were stabilized with a 5 wt. % PVA aqueous solution, and then polymerized at 80 °C for 12 h in a 250 mL

four-neck glass reactor equipped with a mechanical stirrer, a refluxing condenser and a nitrogen injection system. The resulting particles were washed repeatedly using DI water and ethanol. Subsequently, the produced particles were dried under a vacuum at room temperature.

2. 4 Preparation of Highly Monodisperse-Mesoporous Fe₃O₄/C Composite Microspheres

The monodisperse-porous polystyrene microspheres were sulfonated by sulfuric acid treatment because sulfonic acid groups can facilitate carbonization and introduction of Fe₃O₄ dispersed in DI water by applying ultrasonication at room temperature. Two types of iron salts (FeCl₂ and FeCl₃) were dissolved in DI water and were poured into the above DI water containing porous SPS microspheres (equipped with a mechanical stirrer, a refluxing condenser and a nitrogen injection system). The mixture was stirred for 24 h, and then the supernatant containing residual Fe ions was removed by centrifugation. The obtained particles were re-dispersed in DI water for 30 min, and then an aqueous NH₄OH (25 %) solution was added and stirred for 4 h. This reaction mixture was heated at 85 °C for 12 h, and the resulting particles were washed repeatedly using DI water and ethanol. The prepared mesoporous Fe₃O₄/SPS composite microspheres were dried under a vacuum at room temperature. Finally, the mesoporous Fe₃O₄/SPS composite microspheres were heated at 600 °C for 7 h under a nitrogen atmosphere.

2. 5 Particle Characterization

The morphologies of the porous polymer and Fe₃O₄/C composite microspheres were observed by using optical microscopy (OM, Olympus BH-2), scanning electron microscopy (SEM, JSM-6300, JEOL), and focused ion beam-scanning electron microscopy (FIB-SEM). FT-IR spectroscopy (Magna-IR 760 Nicolet) was utilized to analyze the chemical components of the SPS particles. Specific surface area, average pore radius and total pore volume of the porous SPS and mesoporous Fe₃O₄/C composite microspheres were characterized by using the Barrett–Joyner–Halender method (BJH, ASAP2010 Micromeritics). Thermo gravimetric analysis (TGA) was carried out in the temperature range from 30 °C to 900 °C at a heating rate of 5 °C min⁻¹ under an air atmosphere on a SDT2960 (TA Instrument). Magnetite content in the mesoporous Fe₃O₄/C composite microspheres was calculated from the residue. The crystal structures of the mesoporous Fe₃O₄/C composite microspheres were investigated by powder X-ray diffraction experiments conducted in the range from 2θ = 5° to 80°. The carbonized-porous carbon microspheres were characterized by Raman spectroscopy.

2. 6 Electrochemical Test

Electrochemical characterization was performed using coin-type cells (CR-2032). The negative electrode was prepared by coating an N-methyl pyrrolidone (NMP)-based slurry containing mesoporous Fe₃O₄/C composite microspheres, super-P carbon, and polyvinylidene fluoride (PVdF) (7:1:2,

w:w:w) onto a copper foil. The electrodes were dried for 20 min at 110 °C and were not exposed to air before assembly of the cell. Li foil was used as the counter-electrode. The commercial electrolyte consisted of an 1M LiPF₆ salt in a mixture of ethylene carbonate (EC) / diethyl carbonate (DEC) (1:1 by volume, provided by Techno Semichem Co., Ltd., Korea). The charge and discharge rates were calculated assuming the theoretical capacities for Fe₃O₄ (928 mAh g⁻¹) and C (340 mAh g⁻¹).

3. Results and Discussion

3. 1 Characterization of the prepared microspheres

Sample	Conditions
PS-H4	Porous PS microspheres fabricated with 4g of heptane
PS-H7	Porous PS microspheres fabricated with 7g of heptane
SPS-H4	Sulfonated PS-H4
SPS-H7	Sulfonated PS-H7
PC-H4	Carbonized SPS-H4 without Fe ₃ O ₄ nanocrystals
PC-H7	Carbonized SPS-H7 without Fe ₃ O ₄ nanocrystals
FC-H4	Heat treated Fe ₃ O ₄ /SPS-H4 composite microspheres
FC-H7	Heat treated Fe ₃ O ₄ /SPS-H7 composite microspheres

Table 1. List of all samples and a description of particle conditions.

In this study, we controlled the porosities of porous polystyrene (PS) microspheres. First, PS microspheres having different porosities were prepared by seeded polymerization using different amounts of heptane (4g and 7g) as a diluent. The sulfonation of porous PS microspheres was carried out with sulfuric acid to generate porous carbon materials. The list of all samples and description of preparation conditions are summarized in Table 1.

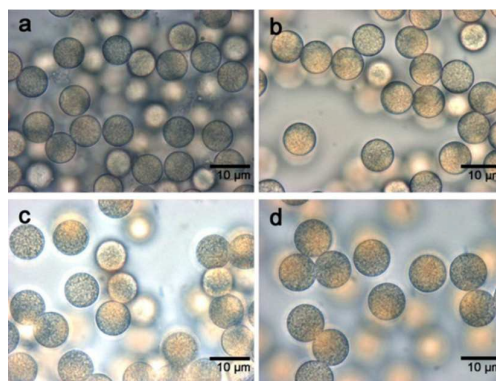


Figure 2. OM images of porous PS microspheres: (a) PS-H4 and (c) PS-H7, and porous PS microspheres after sulfonation: (b) SPS-H4 and (d) SPS-H7.

Figure S1 shows OM and SEM images of polymer particles of each step during the seeded polymerization process. Figure 2 shows optical microscopy (OM) images of PS-H4 (a), PS-H7 (c), SPS-H4 (b) and SPS-H7 (d), which had porous structures and spherical shapes. The average diameters of the porous PS microspheres increased from 7.9 to 9 μm with higher heptane content, as shown in Figs. 2a and c. After sulfonation of PS-H4 and PS-H7, a yellow colored powder was obtained, and their intrinsic shapes were still retained, as shown in Figs. 1b and 1d. Figure S2 shows SEM images of highly monodisperse porous SPS microspheres. The incorporation of SO^3 functional groups to the porous PS microspheres was confirmed by IR spectroscopy measurements.

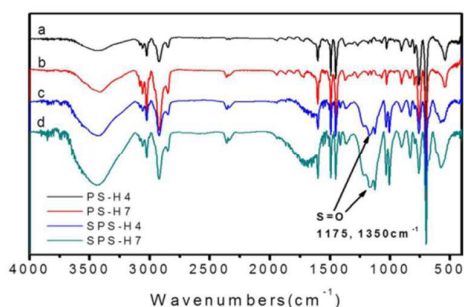


Figure 3. FT-IR spectra of porous PS microspheres: (a) PS-H4 and (b) PS-H7, and sulfonated porous PS microspheres: (c) SPS-H4 and (d) SPS-H7.

Figure 3 shows IR spectra of the porous PS microspheres before (a and b) and after (c and d) sulfonation for 24 h. The porous SPS microspheres have a broad absorption band in the region of 1320–1052 cm^{-1} and a sharp absorption band at 1000 cm^{-1} due to the stretching vibrations from the incorporation of S=O groups, as shown in Figs. 3c and d. The porous PS microspheres were successfully sulfonated by acid treatment using sulfuric acid.

After Fe_3O_4 nanoparticles are formed in SPS microspheres, Fe_3O_4 /SPS composite microspheres were obtained. Figure 4 shows SEM images of the (a) Fe_3O_4 /SPS-H4, (d) Fe_3O_4 /SPS-H7, (b) Fe_3O_4 /C-H4 (FC-H4) and (e) Fe_3O_4 /C-H7 (FC-H7) at low (larger images) and high magnification (insets). After incorporation of Fe ions into the porous SPS microspheres, Fe_3O_4 nanocrystals were formed by a wet chemical reaction in the presence of ammonium hydroxide. The residual clusters consisting of Fe_3O_4 nanocrystals are not observed in Figs. 4a and 4d because the supernatant containing residual Fe ions was removed after introduction of the iron ions into the porous SPS microspheres. Figures 4b and 4e show the carbonized- Fe_3O_4 /SPS-H4 and Fe_3O_4 /SPS-H7, which were heat treated at 600°C for 7 h under a nitrogen atmosphere. Although the average diameters of both samples decreased after heat treating for a long time at a high temperature, as shown in Figs. 4b and 4e, their porous structures were still retained without collapse, as shown in cross-sectional images of Figs. 4c and 4f.

The internal small images of Figs. 4c and 4f are cross-sectional EDX mapping images of FC-H4 and FC-H7, which indicate that Fe_3O_4 nanocrystals are well dispersed in a carbon matrix (yellow colored dots display Fe atoms).

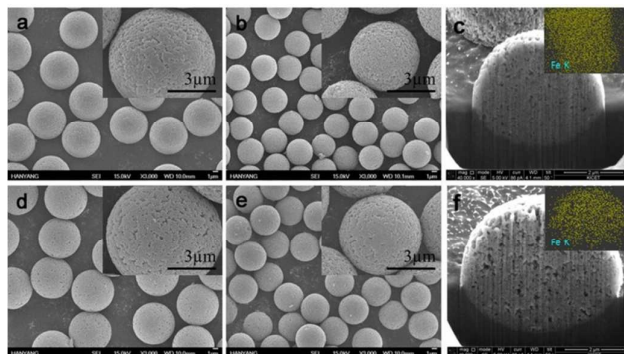


Figure 4. SEM images of mesoporous Fe_3O_4 /SPS composite microspheres (a and d) before and (b and e) after heat treatment in nitrogen atmosphere; (a) Fe_3O_4 /SPS-H4 (b) FC-H4, (d) Fe_3O_4 /SPS-H7 (e) FC-H7, and cross-sectional images of (c) FC-H4 and (f) FC-H7.

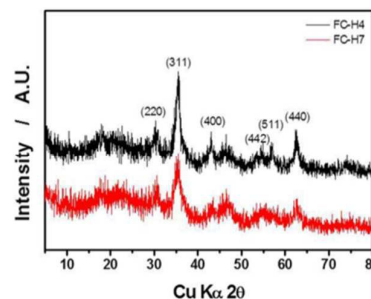


Figure 5. XRD patterns of (black line) FC-H4 and (red line) FC-H7.

Figure 5 shows the XRD patterns of (a) FC-H4 and (b) FC-H7. Both samples show main peaks at $2\theta = 30.09^\circ, 35.43^\circ, 43.00^\circ, 54.07^\circ, 57^\circ$ and 62.5° , which are about the typical XRD peaks of crystalline Fe_3O_4 . Broad peaks corresponding to disordered carbon patterns were observed in the overall region. These results demonstrate that Fe_3O_4 nanocrystals were contained in the disordered carbon matrix, as shown above in cross-sectional mapping images in Figs. 4c and 4f. In addition, it seems that peak broadening of FC-H7 is sufficiently larger than FC-H4. According to this result, it can be estimated by using the (311) peak that crystallite size of Fe_3O_4 contained in FC-H7 is smaller than that of FC-H4.

Figure 6 exhibits nitrogen adsorption-desorption isotherms and BJH pore-size distributions of SPS-H4, SPS-H7, FC-H4 and FC-H7. The distribution in pore size of porous SPS microspheres was relatively broad (10 - 160 nm), as shown insets in Figs. 6a and 6b. However, Fe_3O_4 /C composite microspheres showed a narrow pore-size distribution below 10nm because nano-sized Fe_3O_4 crystals were formed in pores and on the surface of SPS microspheres before carbonization. Nitrogen adsorption-desorption isotherms of the FC-H4 and FC-H7 exhibit isotherms of type IV of the IUPAC classification

featuring a pronounced step due to the capillary condensation and desorption of nitrogen gas, which demonstrates $\text{Fe}_3\text{O}_4/\text{C}$ composite microspheres have large mesopores. Differences in specific surface area, total pore volumes and average pore sizes of SPS-H4, SPS-H7, FC-H4 and FC-H7 analyzed by BET and BJH methods were summarized in Table 2. The total pore volumes of SPS-H4 and SPS-H7 were 0.273 cc g^{-1} and 0.423 cc g^{-1} , respectively. As mentioned above, using more heptane increased the average diameter of the polymerized porous microspheres. The total pore volume of SPS-H7, having similar average pore size to SPS-H4, was larger than that of SPS-H4.

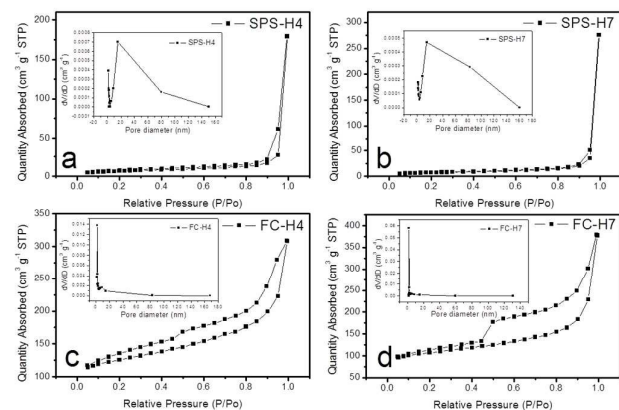


Figure 6. Nitrogen adsorption-desorption isotherms and (insets) BJH pore-size distributions of (a) SPS-H4, (b) SPS-H7, (c) FC-H4 and (d) FC-H7.

Sample	Specific surface area ($\text{m}^2\text{ g}^{-1}$)	Total pore volume (cc g^{-1})	Average pore radius (nm)
SPS-H4	18.5	0.273	15.5
SPS-H7	19.9	0.423	15.4
FC-H4	110.8	0.296	1.9
FC-H7	232.5	0.504	1.9

Table 2. Textural properties of the porous-sulfonated polystyrene (SPS) and $\text{Fe}_3\text{O}_4/\text{C}$ composite microspheres fabricated by using polymer seed particles with different amounts of diluent evaluated from BET and BJH methods.

$\text{Fe}_3\text{O}_4/\text{C}$ composite microspheres showed a dramatic increase of specific surface area due to the nano-sized Fe_3O_4 crystals. Especially, the specific surface areas of FC-H7 increased more than 10 times because of the higher content and smaller crystallite size of Fe_3O_4 formed in pores than those of FC-H4 as mentioned above in Fig. 5. Thermogravimetric analysis (TGA) thermograms of the FC-H4 and FC-H7 are shown in Fig. 7. The TGA measurement was used to reveal the chemical composition of the final composite microspheres. The first weight loss took place at below 200°C , which corresponds to the evaporation of the weakly adsorbed moisture and decomposition of other small molecules like labile oxygen functional groups. Then, the mass of samples slightly increased because of the oxidation of Fe_3O_4 nanocrystals adsorbed onto the surface of the composite microspheres. The rapid weight

loss arose between 380°C and 450°C , which can be attributed to oxidation of carbon with oxygen injected during measurement.

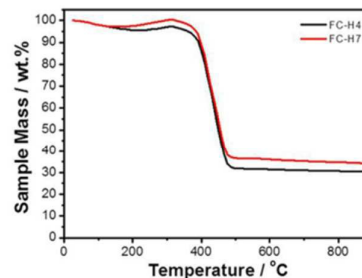


Figure 7. TGA plots of (black line) FC-H4 and (red line) FC-H7 under an air conditions at a heating rate of 5°C min^{-1} .

Although both TGA curves exhibited similar weight loss trends, the FC-H7 had a higher residual weight of 34.8 wt. % than that of 30 wt. % for the FC-H4. This indicates that the porous SPS microspheres, having larger pore volumes could contain a higher content of Fe_3O_4 nanocrystals via a wet chemical method.

In order to compare the electrochemical performance of the $\text{Fe}_3\text{O}_4/\text{C}$ microspheres, porous carbon microspheres without Fe_3O_4 nanocrystals were prepared and their electrochemical properties were confirmed. The morphologies of the black-colored powder and characteristics were confirmed by SEM and Raman spectroscopy, as shown in Figs. S3 and S4. SEM images show two spherical porous carbon spheres with different particle size named PC-H4 and PC-H7. In the Raman spectrum of the PC-H4, the G band was broadened and shifted to 1592 cm^{-1} , and a broad D band at 1336 cm^{-1} also appears. The Raman spectrum of PC-H7 also contained both D and G bands (at 1592 cm^{-1} and 1335 cm^{-1} , respectively). The D/G intensity ratio of the PC-H4 and PC-H7 had values of 0.724 and 0.736. Therefore, the PC-H4 and PC-H7 were composed of hard carbon having graphite and a disordered structure.

All voltage profiles were measured at a 1C-rate except the first two cycles at a 1/20 C rate. The voltage profiles of the (a) PC-H4 and (b) PC-H7 for the first three cycles and 100th cycle are shown in Figure S5. Both the PC-H4 and PC-H7 composite electrodes show a similar staging process evolving at the typical low voltage values where Li-ion insertion occurs in a carbonaceous matrix at the first discharge curve. In the charge process, a similar trend of Li ion extraction is also seen in the first charge curves of the PC-H4 and PC-H7 electrodes. The initial large irreversible capacities (756 and 750 mAh g^{-1}) of both samples are expected phenomena that result from the decomposition of electrolyte and the formation of a solid electrolyte interface (SEI) layer on the surface of active materials. The voltage profiles of the FC-H4 and FC-H7 are shown in Figs. 8a and 8b. Both $\text{Fe}_3\text{O}_4/\text{carbon}$ composite electrodes exhibit similar first discharge curves with a small voltage plateau at around 1.5 V, which can be attributed to the formation of $\text{Li}_x\text{Fe}_3\text{O}_4$ intermediates. The voltage plateau at around 0.8V was also seen in both electrodes, and should be

attributed to the reaction $\text{Fe}_3\text{O}_4 + 8\text{Li}^+ + 8\text{e}^- \leftrightarrow 3\text{Fe}^0 + 4\text{Li}_2\text{O}$. In the first charge process, two small plateaus were observed at about 1.6 V and 1.9 V, corresponding to the oxidation of Fe^0 to Fe^{2+} and Fe^{3+} , respectively [10]. The FC-H4 and FC-H7 composite electrodes show smaller irreversible capacities in the first discharge process and higher reversible capacities at all cycles compared to those of PC-H4 and PC-H7. Figure 7c shows cycling performance of the (inverted triangle) PC-H4, (triangle) PC-H7, (square) FC-H4 and (circle) FC-H7 composite electrodes, tested between 0.02 and 3.0V at the rate of 1/20C (first two cycles) and 1C up to 100 cycles. All electrodes show good cyclability with high efficiency (>99%) at all cycles, as shown in figure 8c. Among all electrodes, the capacity of FC-H7 electrodes was highest, which showed good capacity retention without capacity decay even after 100 cycles at 1C rate.

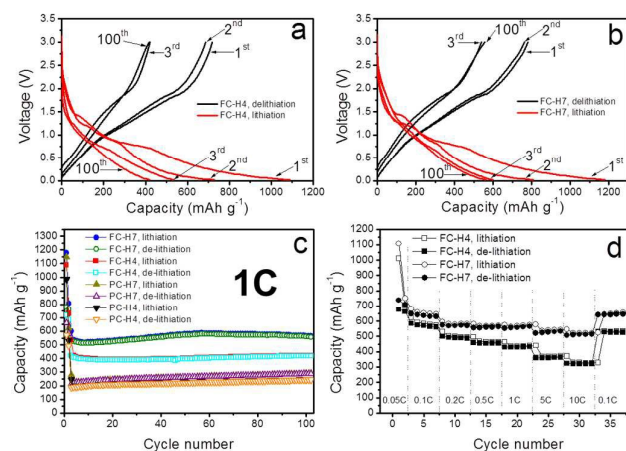


Figure 8. Voltage profiles of (a) FC-H4, (b) FC-H7 composite electrodes in the 0.02-3V voltage window at (first two cycles) 1/5 and (third and 100th cycles) 1C. (c) Cycling performance of (inverted triangle) PC-H4, (triangle) PC-H7, (square) FC-H4 and (circle) FC-H7 composite electrodes in the 0.02-3V voltage window at 1/20 C (first two cycles) and 1C. (d) The specific capacity of (square) FC-H4 and (circle) FC-H7 electrodes as a function of the cycling rate (0.1-10 C).

The higher reversible capacity of FC-H7 than that of the FC-H4 electrode was expected from the larger total pore volume, about two times that of FC-H4, and a higher amount of Fe_3O_4 nanocrystals in the carbon matrix. Although the FC-H4 and FC-H7 electrodes have a large amount of Fe_3O_4 nanocrystals, 30 to 35 wt. %, they exhibit excellent cycle performance because the mesopores in the carbon matrix accommodate the volume variation of nanosized- Fe_3O_4 during electrochemical processes. The rate performance is evaluated by discharging at 0.2C and charging at various current rates in the voltage range of 0.02 – 3.0V and displayed in figure 8d. FC-H4 and FC-H7 electrodes exhibit high capacity at all current rates due to the narrow size distribution and porosity of the $\text{Fe}_3\text{O}_4/\text{C}$ composite microspheres. In particular, the FC-H7 electrode exhibits a higher discharge-charge capacity than that of the FC-H4 electrode because of a higher amount of Fe_3O_4 nanocrystals,

as shown in Fig. 7b. The discharge capacities at different current rates are 642, 570, 565, 563, 529 and 512 mAh g^{-1} at 0.1, 0.2, 0.5, 1, 5 and 10C, respectively. The capacity ultimately returns to above 640 mAh g^{-1} at 0.1C. In addition, the capacity retention is better than that of the FC-H4 electrode with high coulombic efficiency. The higher capacity and better rate capability of the FC-H7 electrode are mainly attributed to more Fe_3O_4 nanocrystals in an amorphous carbon matrix, lots of mesopores and higher specific surface area, as mentioned above. Existing mesopores not only provide the volume for expansion of Fe_3O_4 nanocrystals, but it also allows for more efficient transport of electrons and Li-ions during the lithiation-delithiation processes. To demonstrate the improvement of our $\text{Fe}_3\text{O}_4/\text{C}$ composite materials, we also tested the electrochemical performance of coin-cell made with bare Fe_3O_4 nanoparticles. This bare Fe_3O_4 composite electrode was prepared under the same condition with other electrodes that we made (active material:super-P:binder = 7:1:2, w:w:w). Figure S6 exhibits the (a) cycling performance (1C) and (b) the specific capacity as a function of the various cycling rates (0.1-5C) of bare Fe_3O_4 composite electrode. The discharge capacities were about 30 mAh g^{-1} from third cycle to 100th cycle while the first discharge capacity at 0.05C was about 1500 mAh g^{-1} , as shown in Fig. S6a. The rapid capacity fading was also observed in the C-rate test (Fig. S6b). In light of these results, the porous carbon matrix acts an important role for the prevention of capacity fading.

To understand the textural effect of porous $\text{Fe}_3\text{O}_4/\text{C}$ composite microspheres on the kinetics of the charge- and mass-transfer reaction, the electrochemical impedance spectroscopy (EIS) analysis was performed. Figure 9a shows Nyquist plots of FC-H4 and FC-H7 composite electrodes (red circle and black square) at 100th cycle. The electrochemical system can be modeled by an equivalent circuit as shown in Fig. 9b. Figure 9 exhibited two overlapping semi-circles at high frequency. The high frequency one is attributed to the SEI film resistance (R_{SEI}). The medium frequency one is associated with the double-layer capacitance (C_{dl}) and charge-transfer resistance (R_{ct}) of $\text{Fe}_3\text{O}_4/\text{C}$ composite electrodes. In low frequency, the Warburg-type straight lines show an angle approaching 68.8° and 45.3° to the Z'-axis indicating that the resistance associated the mass transfer depends on the porosity and the surface area of $\text{Fe}_3\text{O}_4/\text{C}$ composite electrodes. According to the fitted values for two types of cells, the radius of semi-circles at medium frequency of FC-H7 composite electrode is smaller than that of FC-H4 composite electrode while the semi-circles at high frequency are similar, which indicated that the charge transfer resistance of FC-H7 (195 Ω) composite cell is smaller than that of the cell made with FC-H4 (268 Ω). Due to the much higher specific surface and larger pore volume which improve electrochemical kinetic characteristics of Li-ions, FC-H7 composite electrode exhibited better capacity retention even at high current rates.

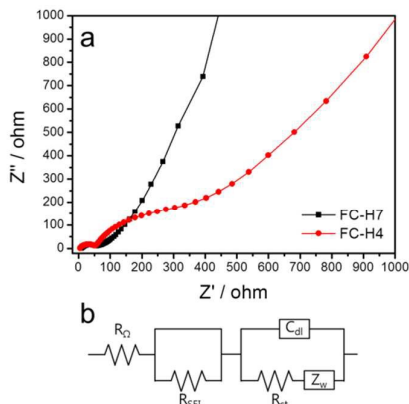


Figure 9. (a) Nyquist plots of (red circle) FC-H4 and (black square) FC-H7 composite electrodes at 100th cycle. (b) The equivalent circuit used to model the impedance spectra.

4. Conclusions

The highly monodisperse porous carbon microspheres containing well-distributed Fe_3O_4 nanocrystals in the pores were fabricated by wet chemical method using porous sulfonated PS (SPS) particles. The sulfonic acid groups of SPS microspheres enable to form Fe_3O_4 nanoparticles in the small pores. The amounts of Fe_3O_4 nanoparticles depend to the total pore volume of SPS microspheres. After heat treatment in a nitrogen atmosphere, the monodisperse mesoporous $\text{Fe}_3\text{O}_4/\text{C}$ composite microspheres with high specific surface area were obtained. The electrochemical performance of the mesoporous $\text{Fe}_3\text{O}_4/\text{C}$ composite microspheres was compared with the porous carbon microspheres without Fe_3O_4 nanocrystals, and bare Fe_3O_4 nanoparticles. Two types of $\text{Fe}_3\text{O}_4/\text{C}$ composite electrodes showed high specific capacity and good capacity retention even at high current rates. There are two important reasons for improved cycle performance of the monodisperse mesoporous $\text{Fe}_3\text{O}_4/\text{C}$ composite microspheres. One is the void and carbon wall of porous carbon microspheres which accommodate the volume change of Fe_3O_4 nanoparticles and prevent the aggregation of Fe_3O_4 nanoparticle. The other one is the monodisperse particles with a uniformity of the porosity which keeps stable electrochemical kinetic characteristics of the cells even at high current rates.

Acknowledgements

This work was supported by a grant from the Human Resources Development Program of KETEP, funded by the Ministry of Trade, Industry and Energy, Korea (No. 20124010203290).

Notes and references

- 1 M. Armand and J. M. Tarascon, *Nature* 2008 **451** 652.
- 2 B. Kang and G. Ceder, *Nature* 2009 **458** 190.
- 3 J.M. Tarascon and M. Armand, *Nature* 2001 **414** 359.
- 4 Z. M. Cui, L. Y. Jiang, W. G. Song and Y. G. Guo, *Chem. Mater.* 2009 **21** 1162.
- 5 L. Wang, Y. Yu, P. C. Chen, D. W. Zhang and C. H. Chen, *J. Power Sources* 2008 **183** 717.
- 6 P. Poizot, S. Laruelle, S. Grugeon, L. Dupont and J.M. Tarascon, *Nature* 2000 **407** 496.
- 7 C. K. Chan, H. L. Peng, G. Liu, K. McIlwrath, X. F. Zhang, R. A. Huggins and Y. Cui, *Nat. Nanotechnol.* 2008 **3** 31.
- 8 D. Deng and J. Y. Lee, *Angew. Chem.* 2009 **121** 1688.
- 9 J. Li, H. M. Dahn, L. J. Krause, D. B. Le and J. R. Dahn, *J. Electrochem. Soc.* 2008 **155** A812.
- 10 P.C. Lian, X.F. Zhu, H.F. Xiang, L. Zhong, W. S. Yang and H. H. Wang, *Electrochim. Acta* 2010 **56** 834.
- 11 W. M. Zhang, X. L. Wu, J. S. Hu, Y. G. Guo and L. J. Wan, *Adv. Funct. Mater.* 2008 **18** 3941.
- 12 T. Muraliganth, A. V. Murugan and A. Manthiram, *Chem. Commun.* 2009 **47** 7360.
- 13 W. M. Zhang, X. L. Wu, J. S. Hu, Y. G. Guo and L. J. Wan, *Adv. Funct. Mater.* 2008 **18** 3941.
- 14 T. Yoon, C. Chae, Y. -K. Sun, X. Zha, H. H. Kung and J. K. Lee, *J. Mater. Chem.* 2011 **21** 17325.
- 15 X. J. Zhang, W. H. Shi, J. X. Zhu, W. Y. Zhao, J. Ma, S. Mhaisalkar, T. L. Maria, Y. H. Yang, H. Zhang, H. H. Hng and Q. Y. Yan, *Nano Research* 2010 **3** 643.
- 16 Y. Z. Piao, H. S. Kim, Y. E. Sung and T. Hyeon, *Chem. Commun.* 2010 **46** 118.
- 17 H. Liu, G.X. Wang, J. Z. Wang and D. Wexler, *Electrochem. Commun.* 2008 **10** 1879.
- 18 J. Chen, L. Xu, W. Li, X. Gou, *Adv. Mater.* 2005 **17** 582.
- 19 J. B. Nam, J. H. Ryu, J. W. Kim, I. S. Chang and K. D. Suh, *Polymer* 2005 **46** 8956.
- 20 J. B. Jun, S. Y. Uhm, J. H. Ryu and K. D. Suh, *Colloids and Surfaces A: Physicochem. Eng. Aspects* 2005 **260** 157.
- 21 A. Magasinski, P. Dixon, B. Hertzberg, A. Kvit, J. Ayala and G. Yushin, *Nature Mater.* 2010 **9** 353.
- 22 B. -Y. Jung, H. -S. Lim, Y. -K. Sun and K. -D. Suh, *J. Power Sources*, 2013 **244** 177.
- 23 J. -W. Kim, J. -H. Ryu and K. -D. Suh, *Colloid. Polym. Sci* 2001 **279** 146.